Smart Structures and Systems, *Vol. 14, No. 6 (2014) 1081-1103*
DOI: http://dx.doi.org/10.12989/sss.2014.14.6.1081

Feedforward actuator controller development using the backward-difference method for real-time hybrid simulation

Brian M. Phillips[*1], Shuta Takada[2a], B.F. Spencer, Jr.[3b] and Yozo Fujino[2c]

[1]*Department of Civil and Environmental Engineering, University of Maryland, College Park, Maryland, USA*
[2]*Department of Civil Engineering, University of Tokyo, Tokyo, Japan*
[3]*Department of Civil and Environmental Engineering, University of Illinois, Urbana, Illinois, USA*

(Received March 15, 2014, Revised June 5, 2014, Accepted June 7, 2014)

Abstract. Real-time hybrid simulation (RTHS) has emerged as an important tool for testing large and complex structures with a focus on rate-dependent specimen behavior. Due to the real-time constraints, accurate dynamic control of servo-hydraulic actuators is required. These actuators are necessary to realize the desired displacements of the specimen, however they introduce unwanted dynamics into the RTHS loop. Model-based actuator control strategies are based on linearized models of the servo-hydraulic system, where the controller is taken as the model inverse to effectively cancel out the servo-hydraulic dynamics (i.e., model-based feedforward control). An accurate model of a servo-hydraulic system generally contains more poles than zeros, leading to an improper inverse (i.e., more zeros than poles). Rather than introduce additional poles to create a proper inverse controller, the higher order derivatives necessary for implementing the improper inverse can be calculated from available information. The backward-difference method is proposed as an alternative to discretize an improper continuous time model for use as a feedforward controller in RTHS. This method is flexible in that derivatives of any order can be explicitly calculated such that controllers can be developed for models of any order. Using model-based feedforward control with the backward-difference method, accurate actuator control and stable RTHS are demonstrated using a nine-story steel building model implemented with an MR damper.

Keywords: hybrid simulation; real-time hybrid simulation; actuator control, backward-difference method

1. Introduction

Experimental testing is an essential tool for understanding how structures respond to extreme dynamic events, thus allowing for the design and construction of safer structures. Hybrid simulation (or pseudodynamic testing) provides an attractive approach for the dynamic testing of structural systems, combining physical testing with numerical simulation (Hakuno *et al*. 1969, Takanashi *et al*. 1975, Mahin and Shing 1985, Takanashi and Nakashima 1987, Mahin *et al*. 1989, Shing *et al*. 1996). Through the technique known as substructuring, the structure of interest can be

*Corresponding author, Assistant Professor, E-mail: bphilli@umd.edu
[a] Ph.D. Student, E-mail: takada@bridge.t.u-tokyo.ac.jp
[b] Professor, E-mail: bfs@illinois.edu
[c] Professor, E-mail: fujino@sogo.t.u-tokyo.ac.jp

http://www.techno-press.org/?journal=sss&subpage=8 ISSN: 1738-1584 (Print), 1738-1991 (Online)

divided into numerical and experimental components; the numerical components are well understood and easy to model while the experimental components may experience complex nonlinear behavior. The numerical components are evaluated using numerical integration and servo-hydraulic actuators maintain compatibility at the interface between numerical and experimental components. Typically, displacements are imposed on the experimental component (i.e., physical specimen) and the corresponding restoring forces are measured and returned to the numerical integration scheme.

When the experimental component has significant rate-dependent behavior, the entire hybrid simulation must be conducted in real-time (i.e., real-time hybrid simulation or RTHS). In RTHS, the servo-hydraulic system introduces unwanted dynamics into the loop of action and reaction. Many actuator control strategies have been proposed to enable accurate and stable RTHS. Early efforts in actuator control focused on a single time delay, lumping together all of the actual time delays and lags present in the RTHS loop (Horiuchi *et al*. 1996). For this reason, early approaches are referred to simply as delay compensation. Note that a pure time delay has a constant, unit gain; thus, these approaches also ignored the frequency-dependent amplitude variation of the servo-hydraulic actuator response.

Because time lags are not constant, but rather frequency and specimen dependent, assuming a single time delay is not adequate to characterize the dynamic behavior of servo-hydraulic actuators. Researchers have begun to address the servo-hydraulic system as a dynamic system, creating low-order transfer functions to represent the dynamics (Jung *et al*. 2007, Wallace *et al*. 2007, Chen and Ricles 2009). Inverses of these models can provide accurate compensation over the frequency range for which the model is accurate. With stiff or MDOF structures, there is a potential for instabilities to manifest due to unmodeled high frequency servo-hydraulic dynamics. These approaches are also heuristic, designed to compensate for an observed time delay or time lag.

Recently, strategies have focused on accurate modeling of the servo-hydraulic system, resulting in a better understanding of the actuator control problem and improved control performance over a broad frequency range (Carrion and Spencer 2007, Carrion *et al*. 2009, Phillips and Spencer 2011, Phillips and Spencer 2012a,b). Such model-based control methods account directly for the frequency-dependent dynamics (both amplitude and phase) of the servo-hydraulic system. These methods require accurate models of the servo-hydraulic system developed through system identification. Accurate linear transfer function models, including the servo-controller with PID loop, servo-valve, actuator, and specimen, typically consist of more poles than zeros. Model-based feedforward controllers, which are designed as model inverses to cancel the modeled dynamics, would thus be improper. In Carrion and Spencer (2007), a low-pass filter is added to the feedforward controller to create a proper and implementable controller. In Phillips and Spencer (2012a), higher-order derivatives of the improper inverse are calculated directly using a linear acceleration extrapolation and central difference equations to avoid adding the unwanted dynamics of a low-pass filter. However, this approach is designed for and limited to servo-hydraulic system models of no zeros and three poles.

This research presents a general approach to developing model-based feedforward controllers for RTHS. A backward-difference method is proposed to calculate the necessary discrete time derivatives to implement an improper inverse for actuator control, providing a simpler and more flexible alternative. The proposed feedforward controller is verified for predefined tracking exercises as well as for a nine-story steel structure in RTHS, both using a large-scale MR damper as the physical specimen.

2. Problem formulation

In RTHS, the equations of motion governing the response of the structure are solved using numerical integration. At each time step, displacements **x** at all degrees-of-freedom (DOF) are calculated. To achieve compatibility between numerical and experimental substructures, the subset of **x** corresponding to the interface $\mathbf{x}^{\mathrm{I}}$ shared between both numerical and experimental components are commanded to the physical specimen using servo-hydraulic actuators as **u**. Inner-loop actuator control provides nominal tracking of the command vector **u** to the servo-hydraulic system as measured by $\mathbf{x}^{\mathrm{E}}$, the vector of interface DOFs physically realized by the experimental component. In this notation, the superscript "I" identifies the interface displacements that the actuators are attempting to track while the superscript "E" identifies the experimental displacements which are physically realized by the actuator. In RTHS, outer-loop actuator control is typically added to determine **u** such that $\mathbf{x}^{\mathrm{E}}$ tracks $\mathbf{x}^{\mathrm{I}}$ very accurately and in real-time. The proposed feedforward controller approach will be explored for a single actuator system (i.e., one interface DOF). Special considerations for multi-actuator systems are investigated in Phillips and Spencer (2012b).

A servo-hydraulic system is an assemblage of mechanical and electrical components used to excite a physical specimen, typically to track a prescribed displacement. Individual component models can be assembled to create a dynamic model for the complete servo-hydraulic system, such as in Fig. 1. Components with nonlinear behavior will be represented by linear models with respect to an operating point such that the complete system model is also linear. The linear model will facilitate the use of frequency domain techniques including the Laplace transform as well as frequency domain based system identification.

The flow of oil through the actuator chambers can be approximated by the following linearization (Merritt 1967)

$$Q_{\mathrm{L}} = K_{\mathrm{q}}^{'} x_{\mathrm{v}} - K_{\mathrm{c}}^{'} p_{\mathrm{L}} \tag{1}$$

where Q_{L} is the oil flow through the load, $K_{\mathrm{q}}^{'}$ is the valve flow gain, x_{v} is the position of the valve spool, $K_{\mathrm{c}}^{'}$ is the valve flow-pressure gain, and p_{L} is pressure drop across the load. The system in Eq. (1) has been linearized about the origin where $Q_{\mathrm{L}} = 0$, $x_{\mathrm{v}} = 0$, and $p_{\mathrm{L}} = 0$.

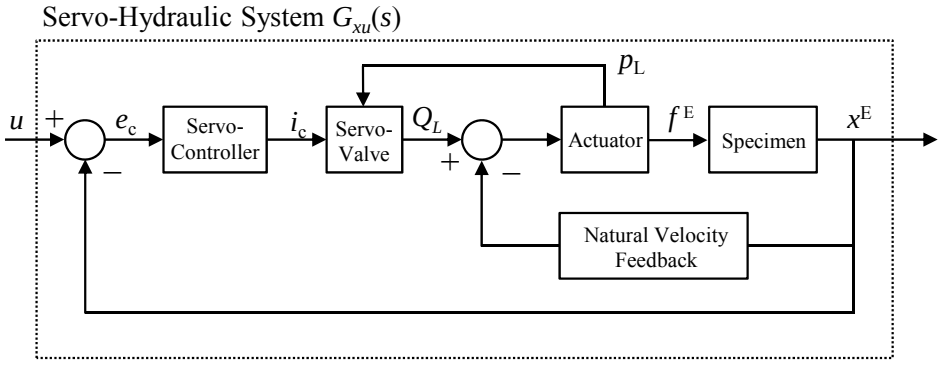

Fig. 1 Components of the servo-hydraulic system

The behavior of the actuator can be described by force equilibrium of the flow rate (Merritt, 1967)

$$Q_{\mathrm{L}} = A\dot{x} + C_{\mathrm{l}} p_{\mathrm{L}} + \frac{V_{\mathrm{t}}}{4\beta_{\mathrm{e}}} \dot{p}_{\mathrm{L}} \tag{2}$$

where C_{l} is the total leakage coefficient of the actuator piston, V_{t} is the total volume of fluid under compression in both actuator chambers, β_{e} is the effective bulk modulus of the system, and *A* is the area of the actuator piston.

The force generated by the actuator f^{E} and thus imparted on the specimen is given by

$$f^{\mathrm{E}} = Ap_{\mathrm{L}} \tag{3}$$

The specimen is excited by the actuator, moving due to the applied force. The equation of motion of the specimen (assuming a linear, single-degree-of-freedom specimen) is given by

$$m^{\mathrm{E}}\ddot{x}^{\mathrm{E}} + c^{\mathrm{E}}\dot{x}^{\mathrm{E}} + k^{\mathrm{E}}x^{\mathrm{E}} + F_{\mathrm{s}} = f^{\mathrm{E}} \tag{4}$$

where m^{E}, c^{E}, and k^{E} represent the mass, damping, and stiffness values of the specimen and attachments (which may include the piston rod, load cell, clevis, etc.), F_{S} represents the friction in the piston rod, x^{E} represents the displacement of the specimen, and dots indicate differentiation with respect to time. Modern actuators often use low-friction seals such that the friction force can be assumed negligible.

The servo-controller is used to stabilize the inherently unstable hydraulic actuator. With displacement feedback, the error signal e_{c} is equal to the difference between the command *u* and measured displacement x^{E}.

$$e_{\mathrm{c}} = u - x^{\mathrm{E}} \tag{5}$$

Servo-controllers often use PID control to eliminate the error. For real-time applications, proportional gain alone is generally adequate, avoiding the lag introduced by integral control and sensitivity to noise of derivative control. With a proportional controller, the servo-controller dynamics can be expressed as

$$i_{\mathrm{c}} = K_{\mathrm{P}} e_{\mathrm{c}} \tag{6}$$

where K_{P} is the proportional feedback gain of the servo-controller and i_{c} is the command signal to the servo-valve.

The servo-valve provides an interface between the electrical and mechanical components of the system. The servo-valve receives an electrical signal from the servo-controller which moves the position of the valve spool, controlling the flow of oil into the actuator. A constant gain k_{v} may be used to approximate the servo-valve dynamics over low-frequency ranges (Merritt 1967, Dyke *et al.* 1995, Carrion and Spencer 2007).

The components of the servo-hydraulic system can be combined into the block diagram model of Fig. 2 with the actuator and specimen represented in the Laplace domain.

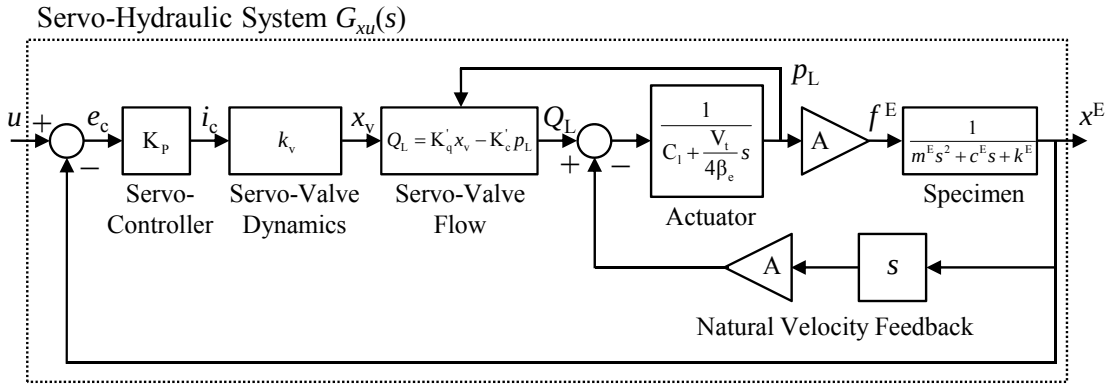

Fig. 2 Block diagram model of the servo-hydraulic system

The servo-hydraulic system model of Fig. 2 can be represented by the following three-pole transfer function

$$G_{xu}(s) = \frac{K_P \frac{K_q A}{K_c}}{\left(\frac{V_t}{4\beta_e K_c} m^E\right)s^3 + \left(m^E + \frac{V_t}{4\beta_e K_c} c^E\right)s^2 + \left(c^E + \frac{V_t}{4\beta_e K_c} k^E + \frac{A^2}{K_c}\right)s + \left(k^E + K_P \frac{K_q A}{K_c}\right)} \tag{7}$$

where $K_q = K_q' k_v$ is the servo-valve gain and $K_c = K_c' C_l$ is the total flow-pressure coefficient. The proposed model-based feedforward control strategy is developed for a general servo-hydraulic system model, but at the same time informed by the knowledge that the model will likely follow a form similar to Eq. (7). Furthermore, it is expected for practical RTHS that the specimen conditions are unknown and nonlinear. The specimen conditions, namely the specimen's influence on actuator control, are determined indirectly through non-parametric servo-hydraulic system identification as described in Section 5. Nonlinearities will be accommodated by the proposed actuator control technique through the feedback controller.

3. Model-based actuator control

In model-based control, an outer-loop controller is created to cancel out the dynamics of the servo-hydraulic system and reduce tracking error (Carrion and Spencer 2007, Phillips and Spencer 2011). The tracking error between the desired and measured displacement (or x^I and x^E, respectively) is given by

$$e = x^I - x^E \tag{8}$$

The model-based controller incorporating both feedforward and feedback links is represented schematically in Fig. 3. The servo-hydraulic system of Fig. 1 has been condensed to show the details of the model-based controller, which acts as an outer-loop controller around the system.

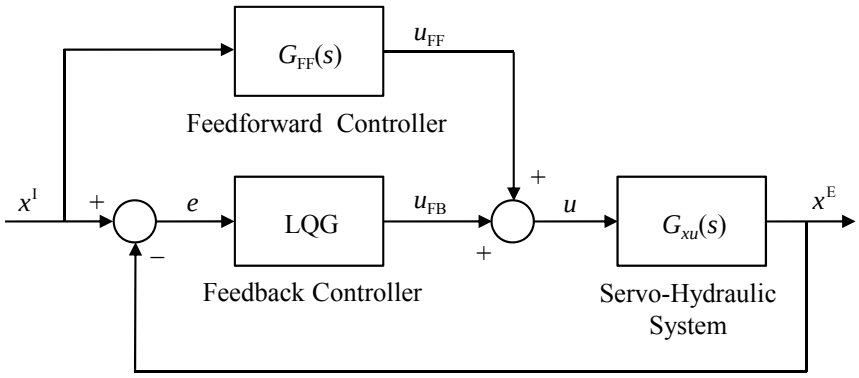

Fig. 3 Model-based actuator control withfeedforward and feedback links

The development of the feedforward and feedback links for model-based control will be presented for a general case.

3.1 Feedforward controller

The feedforward controller is designed to cancel the modeled dynamics of the servo-hydraulic system. In general, the servo-hydraulic system can be represented by the following transfer function model

$$G_{xu}(s) = \frac{X^{E}(s)}{U(s)} = \frac{b_0 + b_1 s + \cdots + b_m s^m}{a_0 + a_1 s + \cdots + a_n s^n} \tag{9}$$

For the model in Eq. (9), the feedforward controller can be expressed as the inverse, or

$$G_{FF}(s) = \frac{U_{FF}(s)}{X^{I}(s)} = \frac{a_0 + a_1 s + \cdots + a_n s^n}{b_0 + b_1 s + \cdots + b_m s^m} \tag{10}$$

For an accurate model of a servo-hydraulic system, the number of poles is generally larger than the number of zeros, as was shown for the model in Eq. (7).

3.1.1 Proper versus improper inverses

If Eq. (10) is both proper and stable, meaning $m \geq n$ and all poles are stable, then the feedforward controller can be implemented without modification. For use with a digital controller, a discrete time approximation such as pole-zero matching or Tustin's method may be used.

If $m < n$, the feedforward controller is improper and requires modification. A low-pass filter could be added to Eq. (10) to reduce the degree to which the inverse is improper. With enough poles, the low-pass filter could even create a proper system (Carrion and Spencer 2007)

$$G_{FF}(s) = \frac{a_0 + a_1 s + \cdots + a_n s^n}{b_0 + b_1 s + \cdots + b_m s^m} \cdot \frac{1}{c_0 + c_1 s + \cdots + c_{n-m} s^{n-m}} \tag{11}$$

where c_0 through c_{n-m} are the coefficients of the low-pass filter. However, low-pass filters canintroduce unwanted dynamics into the feedforward controller. The approach proposed herein for accommodating the improper transfer function is to make use of higher-order derivatives which are available from numerical integration during RTHS. The improper feedforward model of Eq. (10) can be separated into proper and improper terms

$$G_{\mathrm{FF}}(s)=\frac{a_0+a_1s+\cdots+a_ms^m}{b_0+b_1s+\cdots+b_ms^m}+\frac{a_{n-m}s^m}{b_0+b_1s+\cdots+b_ms^m}s+\cdots+\frac{a_ns^m}{b_0+b_1s+\cdots+b_ms^m}s^{n-m} \tag{12}$$

Eq. (12) can be expressed in the time domain as

$$u_{\mathrm{FF}}(t)=\frac{a_0+a_1s+\cdots+a_ms^m}{b_0+b_1s+\cdots+b_ms^m}r(t)+\frac{a_{n-m}s^m}{b_0+b_1s+\cdots+b_ms^m}\dot{r}(t)+\cdots+\frac{a_ns^m}{b_0+b_1s+\cdots+b_ms^m}r(t)^{(n-m)} \tag{13}$$

For example, if $m = 0$ and $n = 3$, the feedforward controller could be written as

$$u_{\mathrm{FF}}(t)=\frac{a_0}{b_0}r(t)+\frac{a_1}{b_0}\dot{r}(t)+\frac{a_2}{b_0}\ddot{r}(t)+\frac{a_3}{b_0}\dddot{r}(t) \tag{14}$$

Or if $m = 2$ and $n = 5$,

$$u_{\mathrm{FF}}(t)=\frac{a_0+a_1s+a_2s^2}{b_0+b_1s+b_2s^2}r(t)+\frac{a_3s^2}{b_0+b_1s+b_2s^2}\dot{r}(t)+\frac{a_4s^2}{b_0+b_1s+b_2s^2}\ddot{r}(t)+\frac{a_5s^2}{b_0+b_1s+b_2s^2}\dddot{r}(t) \tag{15}$$

For implementation with a digital controller, the proper components can be discretized using any standard method (i.e., pole-zero matching or Tustin's method) and the higher-order derivatives (from improper components) can be calculated at each time step using information from the numerical integration. Also, in some other applications, the desired trajectory is known a priori (e.g., earthquake motion reproduction on shaking tables); for such cases, smooth derivatives can be created offline.

3.1.2 Positive zeros

If the servo-hydraulic system of Eq. (9) contains zeros with a positive real component (right half-plane zeros), the resulting inverse of Eq. (10) would be unstable due to positive poles. The most straightforward solution is to create the best possible model without the use of right half-plane zeros, avoiding stability concerns in the inverse. In the case that right half-plane zeros cannot be avoided, a zero phase error tracking controller (ZPETC) can be applied to the feedfoward controller (Tomizuka 1987) for RTHS. First, the system model is described by numerator and denominator polynomials

$$G_{xu}(s)=\frac{n(s)}{d(s)} \tag{16}$$

with inverse (feedforward controller) given by

$$G_{\mathrm{FF}}(s)=\frac{d(s)}{n(s)} \tag{17}$$

The feedforward controller poles should be separated into acceptable (negative) and unacceptable (positive) poles, indicated by subscripts "a" and "u", respectively.

$$G_{\mathrm{FF}}(s)=\frac{d(s)}{n_{\mathrm{a}}(s)n_{\mathrm{u}}(s)} \tag{18}$$

The unacceptable poles are then removed by setting the Laplace variable to zero which also maintains the correct DC gain

$$G_{\mathrm{FF}}(s)=\frac{d(s)}{n_{\mathrm{a}}(s)n_{\mathrm{u}}(0)} \tag{19}$$

To maintain the same phase as the original unstable controller, the following adjustment is made

$$G_{\mathrm{FF}}(s)=\frac{d(s)n_{\mathrm{u}}^{*}(s)}{n_{\mathrm{a}}(s)\left[n_{\mathrm{u}}(0)\right]^{2}} \tag{20}$$

where * indicates the complex conjugate. From Eq. (20), it can be seen that an unacceptable inverse pole will lead to an additional zero in the feedforward controller. The ZPETC approach matches the phase of the improper inverse, but distorts magnitude at higher frequencies. The magnitude distortion may negate the benefit of increased model accuracy found by the inclusion of positive zeros. Note that for the servo-hydraulic system explored in this paper, positive zeros were not necessary to fit an accurate model, as can be seen in Eq. (7). When positive zeros are necessary or help improve model accuracy, Eq. (20) can be used.

3.2 Feedback controller

When mechanical actuators are used to excite a specimen, strong dynamic coupling is usually present between the actuator and specimen, identified as control-structure interaction (CSI). This phenomenon was observed and explained by Dyke *et al.* (1995). When specimens undergo changes in behavior (e.g., through damage), the dynamics of the servo-hydraulic system will change through CSI (see Fig. 1). In such cases, actuator control schemes tuned to one specimen condition may no longer be effective.

A feedback controller is added to complement the feedforward controller (see Fig. 3), providing robustness in the presence of changing specimen conditions, modeling errors, and disturbances. A state-space model of the servo-hydraulic system in Eq. (9) is used to develop a model-based LQG feedback controller as in Phillips and Spencer (2011). The proposed feedforward controller will incorporate this LQG feedback controller when mentioned.

4. Feedforward controller implementation

The proposed model-based feedforward actuator control strategy will be examined for a single-actuator system. The parameterized servo-hydraulic system model presented in Eq. (7) will be used as an example to introduce the feedforward controller. The model contains no zeros and three poles

$$G_{xu}(s) = \frac{k_a k_s}{m^E s^3 + \left(-p_a m^E + c^E\right)s^2 + \left(-p_a c^E + A k_a + k^E\right)s + \left(-p_a k^E + k_a k_s\right)} \tag{21}$$

where

$$k_{\mathrm{a}} = \frac{4\beta_{\mathrm{e}} A}{V_{\mathrm{t}}}, \qquad p_{\mathrm{a}} = -\frac{4\beta_{\mathrm{e}}}{V_{\mathrm{t}} K_{\mathrm{c}}}, \qquad k_{\mathrm{s}} = K_{\mathrm{p}} K_{\mathrm{q}}$$

The feedforward controller is taken as the inverse of servo-hydraulic system

$$G_{\mathrm{FF}}(s) = \left(m^{\mathrm{E}} s^2 + c^{\mathrm{E}} s + k^{\mathrm{E}}\right)\frac{(s - p_{\mathrm{a}})}{k_{\mathrm{a}} k_{\mathrm{s}}} + \frac{sA}{k_{\mathrm{s}}} + 1 \tag{22}$$

The feedforward controller can be rewritten as

$$G_{\mathrm{FF}}(s) = a_0 + a_1 s + a_2 s^2 + a_3 s^3 \tag{23}$$

where the coefficients a_0 through a_3 can be determined by expanding Eq. (22). The feedforward controller is improper by three degrees. In the time domain, Eq. (23) becomes

$$u_{\mathrm{FF}}(t) = a_0 x^{\mathrm{I}}(t) + a_1 \dot{x}^{\mathrm{I}}(t) + a_2 \ddot{x}^{\mathrm{I}}(t) + a_3 \dddot{x}^{\mathrm{I}}(t) \tag{24}$$

where dots denote differentiation with respect to time and, as before, "I" refers to the interface DOF. Note that the accelerations (and all other signals) must be in relative coordinates such that they describe the desired trajectory of the physical specimen. In general, the equations of motion are solved at time step $i - 1$ for the displacements at time step i (i.e., time-stepping numerical integration) and the displacements are imposed on the physical specimen. In discrete time, Eq. (24) can be written as

$$u_{\mathrm{FF},i} = a_0 x_i^{\mathrm{I}} + a_1 \dot{x}_i^{\mathrm{I}} + a_2 \ddot{x}_i^{\mathrm{I}} + a_3 \dddot{x}_i^{\mathrm{I}} \tag{25}$$

The feedforward controller for this example actuator model requires the calculation of displacement, velocity, acceleration, and jerk (derivative of the acceleration) at time step i; however, most numerical integration schemes are only explicit in displacement (i.e., only the desired displacement x_i^{I} is known).

Two methods for calculating the necessary higher-order derivatives are presented, including the central difference method (CDM) with linear acceleration extrapolation (Phillips and Spencer 2012a) and proposed the backward-difference method (BDM). Note that these methods are proposed simply to estimate the higher-order derivatives at the required time step and can be selected independently of the numerical integration scheme. In addition to these two methods, a discrete model fitting approach is proposed as an alternative to avoid the need for estimating higher-order derivatives.

The implementation of the feedforward controllers in conjunction with an explicit numerical integration scheme is illustrated in Fig. 4. At each time step, the actuator command is sent to the servo-controller and restoring force measured. Between each time step, numerical integration is performed and the actuator command is determined.

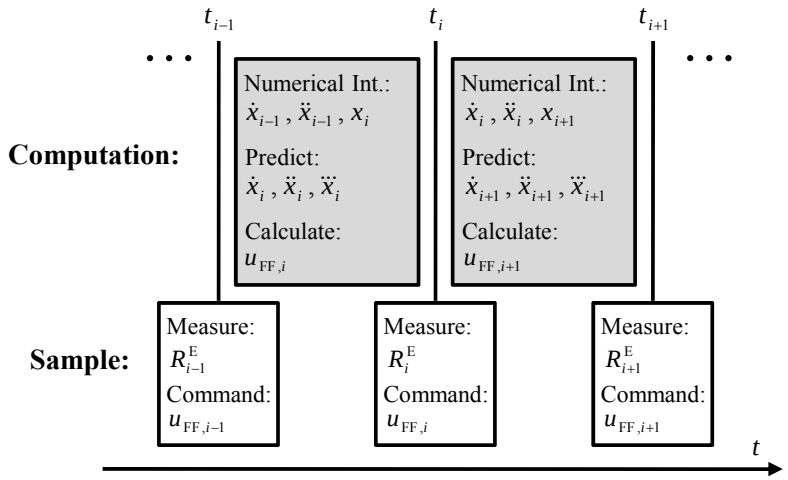

Fig. 4 Implementation of proposed actuator controller in discrete time

4.1 Central difference method with linear acceleration extrapolation

The CDM with linear acceleration extrapolation is designed specifically for a no-zero three-pole servo-hydraulic system model as in Eq. (7) (Phillips and Spencer 2012a). In the CDM, the velocity and acceleration are calculated using the following second order central difference equations

$$\dot{x}_i = \frac{x_{i+1} - x_{i-1}}{2\Delta t} \tag{26}$$

$$\ddot{x}_i = \frac{x_{i+1} - 2x_i + x_{i-1}}{\Delta t^2} \tag{27}$$

To implement the central-difference equations, the desired acceleration is linearly extrapolated over one time step

$$\ddot{x}^{\mathrm{I}}_i = 2\ddot{x}^{\mathrm{I}}_{i-1} - \ddot{x}^{\mathrm{I}}_{i-2} \tag{28}$$

The desired velocity can be computed using Eq. (29), which can be derived from Eqs. (26) and (27).

$$\dot{x}^{\mathrm{I}}_i = \dot{x}^{\mathrm{I}}_{i-1} + \frac{\Delta t}{2}\left(\ddot{x}^{\mathrm{I}}_{i-1} + \ddot{x}^{\mathrm{I}}_i\right) \tag{29}$$

Because a linear extrapolation of the acceleration is chosen, the jerk is calculated as the slope of the extrapolation

$$\dddot{x}^{\mathrm{I}}_i = \frac{1}{\Delta t}\left(\ddot{x}^{\mathrm{I}}_{i-1} - \ddot{x}^{\mathrm{I}}_{i-2}\right) \tag{30}$$

By plugging Eqs. (28)-(30) into Eq. (25), the feedforward controller using the CDM and a linear acceleration extrapolation can be expressed explicitly as

$$u_{\mathrm{FF},i} = Ax_i^{\mathrm{I}} + Bx_{i-1}^{\mathrm{I}} + Cx_{i-2}^{\mathrm{I}} + Dx_{i-3}^{\mathrm{I}} \tag{31}$$

where

$$A = \left[a_0 + \frac{2a_1}{\Delta t} + \frac{2a_2}{\Delta t^2} + \frac{a_3}{\Delta t^3} \right], B = \left[\frac{-7a_1}{2\Delta t} + \frac{-5a_2}{\Delta t^2} + \frac{-3a_3}{\Delta t^3} \right],$$
$$C = \left[\frac{2a_1}{\Delta t} + \frac{4a_2}{\Delta t^2} + \frac{3a_3}{\Delta t^3} \right], D = \left[\frac{-a_1}{2\Delta t} + \frac{-a_2}{\Delta t^2} + \frac{-a_3}{\Delta t^3} \right]$$

Or, as a discrete-time transfer function

$$G_{\mathrm{FF}}(z) = A + Bz^{-1} + Cz^{-2} + Dz^{-3} \tag{32}$$

4.2 Backward-difference method

The method presented in the previous section for calculating higher order derivatives is based on the CDM and linear extrapolation. This method has some limitations; the main one being there is no framework to estimate derivatives beyond the jerk, which may be necessary to implement higher-order feedforward controllers. Also, the technique used to calculate higher order derivatives is not consistent from one derivative to the other.

The proposed feedforward controller employs the backward-difference method to obtain future higher order derivatives, providing a simpler and more general framework for controller development, making it more flexible for a wider range of models. The proposed method is derived from the Taylor series expansion about x_i to obtain $x_{i\text{-}1}$.

$$x_{i-1} = x_i - \dot{x}_i \Delta t + \ddot{x}_i \frac{\Delta t^2}{2} - \dddot{x}_i \frac{\Delta t^3}{6} + \ldots + (-1)^n x_i^{(n)} \frac{\Delta t^n}{n!} + O\left(\Delta t^{n+1}\right) \tag{33}$$

where $O(\Delta t^{n+1})$ is the error term due to truncation of the Taylor series expansion, resulting in a n-th order approximation of derivatives (i.e., error proportional to Δt^n). Note that there are two distinct "orders" when discussing the BDM: the order of the BDM approximation and the order of the derivative that is being calculated.

Derivatives from the first to fourth order are presented in Table 1 using BDM approximations from the first to third order, all derived from Eq. (33).

As an example, a second order BDM approximation can be plugged into Eq. (25) to result in the following discrete-time feedforward controller

$$u_{\mathrm{FF},i} = Ax_i^{\mathrm{I}} + Bx_{i-1}^{\mathrm{I}} + Cx_{i-2}^{\mathrm{I}} + Dx_{i-3}^{\mathrm{I}} + Ex_{i-4}^{\mathrm{I}} \tag{34}$$

where

$$A = \left[a_0 + \frac{3a_1}{2\Delta t} + \frac{2a_2}{\Delta t^2} + \frac{5a_3}{2\Delta t^3} \right], B = \left[\frac{-2a_1}{\Delta t} + \frac{-5a_2}{\Delta t^2} + \frac{-9a_3}{\Delta t^3} \right]$$

$$C = \left[\frac{a_1}{2\Delta t} + \frac{4a_2}{\Delta t^2} + \frac{12a_3}{\Delta t^3} \right], D = \left[\frac{-a_2}{\Delta t^2} + \frac{-7a_3}{\Delta t^3} \right], E = \left[\frac{3a_3}{2\Delta t^3} \right]$$

Or, as a discrete-time transfer function

$$G_{\mathrm{FF}}(z) = A + Bz^{-1} + Cz^{-2} + Dz^{-3} + Ez^{-4} \tag{35}$$

Table 1 Calculation of first to fourth order derivatives for first to third order BDM approximations

	First Order BDM	*Second Order BDM*	*Third Order BDM*
$\dot{x}_i$	$\frac{(x_i - x_{i-1})}{\Delta t}$	$\frac{(3x_i - 4x_{i-1} + x_{i-2})}{2\Delta t}$	$\frac{(11x_i - 18x_{i-1} + 9x_{i-2} - 2x_{i-3})}{6\Delta t}$
$\ddot{x}_i$	$\frac{(x_i - 2x_{i-1} + x_{i-2})}{\Delta t^2}$	$\frac{(2x_i - 5x_{i-1} + 4x_{i-2} - x_{i-3})}{\Delta t^2}$	$\frac{\begin{pmatrix}32x_i - 104_{i-1} + 114x_{i-2} \\ -56x_{i-3} + 11x_{i-4}\end{pmatrix}}{12\Delta t^2}$
$\dddot{x}_i$	$\frac{(x_i - 3x_{i-1} + 3x_{i-2} - x_{i-3})}{2\Delta t^3}$	$\frac{\begin{pmatrix}5x_i - 18x_{i-1} + 24x_{i-2} \\ -14x_{i-3} + 3x_{i-4}\end{pmatrix}}{2\Delta t^3}$	$\frac{\begin{pmatrix}17x_i - 71x_{i-1} + 118x_{i-2} \\ -98x_{i-3} + 41x_{i-4} - 7x_{i-5}\end{pmatrix}}{4\Delta t^3}$
$x_i^{(4)}$	$\frac{\begin{pmatrix}x_i - 4x_{i-1} + 6x_{i-2} \\ -4x_{i-3} + x_{i-4}\end{pmatrix}}{\Delta t^4}$	$\frac{\begin{pmatrix}3x_i - 14x_{i-1} \\ +26x_{i-2} - 24x_{i-3} \\ +11x_{i-4} - 2x_{i-5}\end{pmatrix}}{\Delta t^4}$	$\frac{\begin{pmatrix}35x_i - 186x_{i-1} + 411x_{i-2} \\ -484x_{i-3} + 321x_{i-4} \\ -114x_{i-5} + 17x_{i-6}\end{pmatrix}}{6\Delta t^4}$

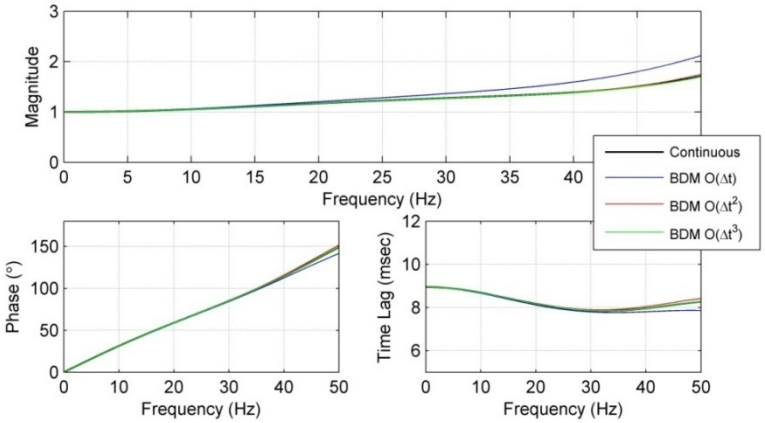

Fig. 5 Feedforward controllers using the BDM approach for various orders of accuracy

To compare the performance of discrete-time feedforward controller implementations, the parameters of Eq. (25) are taken as: $a_0 = 1.000$, $a_1 = 8.950\times10^{-3}$, $a_2 = 2.497\times10^{-5}$, and $a_3 = 6.210\times10^{-8}$. A BDM based feedforward controller is created from first, second, and third order approximations, with the resulting controllers presented in Fig. 5. The corresponding continuous time feedforward controller of Eq. (23) is also presented. From the figure, it is clear that a second or third order approximation necessary for accuracy over the frequency range of 0 to 50 Hz.

The CDM with linear acceleration extrapolation and BDM method (second order) are compared to the continuous time transfer function in Fig. 6 for multiple sampling rates. For both methods, the discrete time approximation approaches the continuous time model as the sampling rate increases. For a given sampling rate, the BDM is more accurate over the frequency range of interest, however requires one more data point for the calculation of the actuator command.

4.3 Discrete model fitting

Examining Eq. (31) and (34), the discrete time improper feedforward controllers can be seen as a model-based extrapolation. That is, a series of previous displacement commands are used to extrapolate future displacements with coefficients determined by the servo-hydraulic system model. Therefore, rather than discretizing a continuous time model, the transfer function model could be directly fit in discrete time by adjusting the parameters a_0 through a_n in:

$$G_{\mathrm{FF}}(z) = a_0 + a_1 z^{-1} + a_2 z^{-2} + \cdots + a_n z^{-n} \tag{36}$$

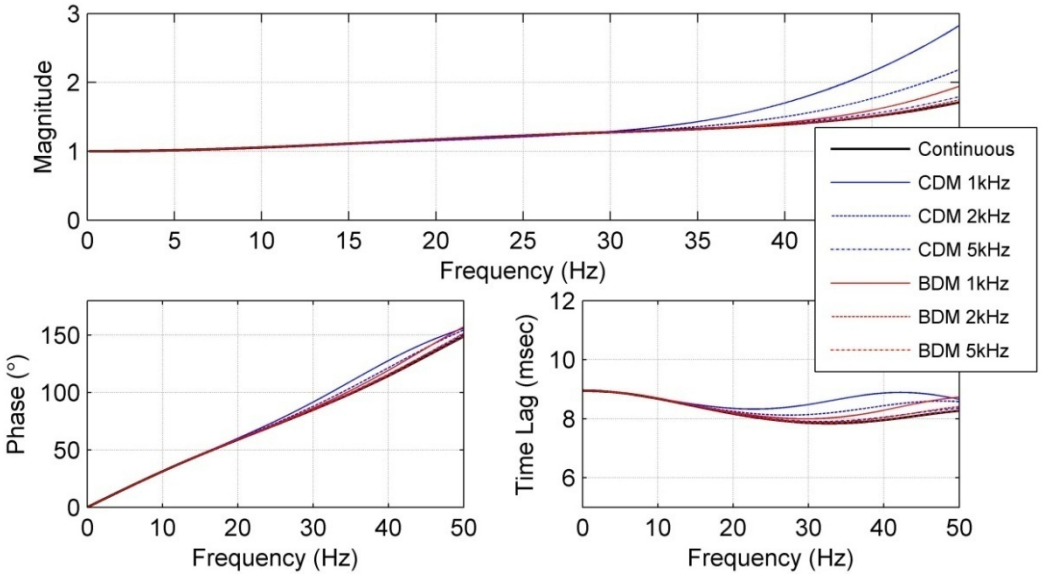

Fig. 6 Feedforward controllers using the CDM and BDM approaches for various sample rates

More generally, the transfer function could be directly fit as a discrete time system with both poles and zeros

$$G_{\mathrm{FF}}(z)=\frac{a_0+a_1z^{-1}+a_2z^{-2}+\cdots+a_nz^{-n}}{b_0+b_1z^{-1}+b_2z^{-2}+\cdots+b_mz^{-m}} \tag{37}$$

The discrete model fitting approach is a general method to develop a feedforward controller and was found to result in similar controllers as the CDM and BDM approaches with additional effort required to optimize the parameters of Eqs. (36) and (37).

5. Experimental evaluation

To evaluate the proposed feedforward control approach, experiments were conducted with both predefined displacements as well as for a complete structure through RTHS. The RTHS testing framework at the University of Illinois located in the Newmark Structural Engineering Laboratory (NSEL, http://nsel.cee.illinois.edu) and part of the Smart Structures Technology Laboratory (SSTL, http://sstl.cee.illinois.edu) is chosen for evaluation. The servo-hydraulic system hardware is shown in Fig. 7. This setup has proven successful for the dynamic testing of large-scale MR dampers (Yang *et al.* 2002, Phillips *et al.* 2010, Phillips and Spencer, 2011).

The actuator, manufactured by the Shore Western Corporation, is rated at 556 kN (125 kips) with a stroke of ±152.4 mm (±6 in), has an effective piston area of 271 cm^2 (42 in^2), and is double ended to provide equal performance both extending and retracting. A Shore Western model 1104 digital servo-controller is used to control the actuator in displacement feedback mode. The displacement of the actuator is measured using an internal AC LVDT. A 445 kN (100 kip) Key Transducers, Inc. model 1411-114-02 load cell is mounted in line with the actuator, measuring the restoring force of the attached specimen.

The RTHS is controlled by a dSPACE model 1103 digital-signal-processor board with a PPC 750GX processor. This board is used to perform numerical integration of the equations of motion for the numerical substructure, apply the outer-loop actuator controller, and control the MR damper current based on semi-active control algorithms.

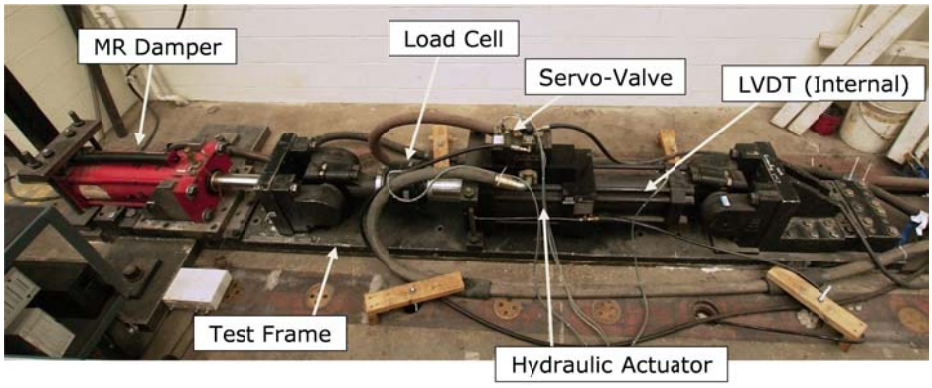

Fig. 7 Experimental setup of the physical specimen

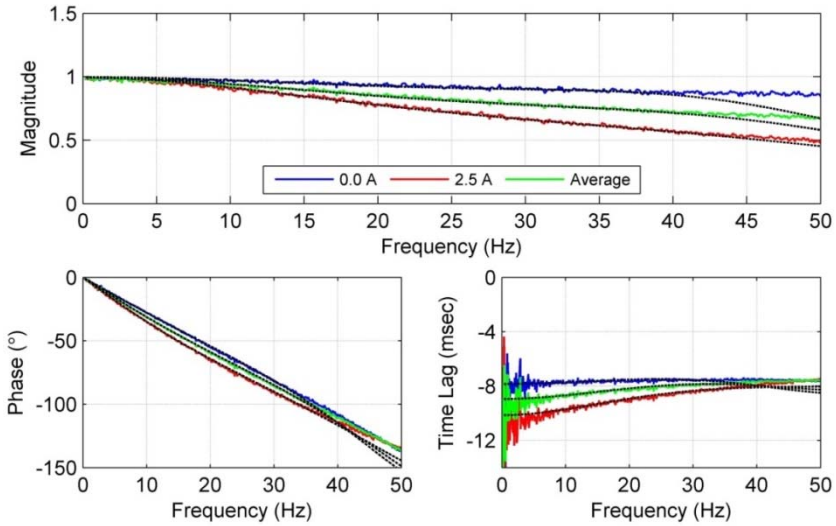

Fig. 8 Measured displacement transfer functions at select current levels

The specimen is a second-generation, large-scale 200 kN MR damper manufactured by the Lord Corporation. The damper has a stroke of ±292 mm (±13 in) and can generate forces slightly higher than the nominal 200 kN. The unique properties of MR dampers are derived from the internal MR fluid. In the presence of a magnetic field, the fluid changes from a linear viscous fluid to a semi-solid with controllable yield strength (Carlson and Jolly 2000). The source of the magnetic field is an electromagnet located in the piston head, excited by an external current which can vary as required by a structural control algorithm. The current in the MR damper circuit is measured using a Tektronix current probe.

System identification of the servo-hydraulic system (Fig. 1) with the MR damper specimen is performed using a band-limited white noise (BLWN) command to the servo-controller with a RMS value of 0.254 mm and a frequency range of 0 to 50 Hz. Because the current to the MR damper can change during the RTHS, the servo-hydraulic dynamics are investigated at multiple current levels. The measured displacement transfer function magnitude, phase, and time lag are presented in Fig. 8 for two conditions: 0.0 and 2.5 Amps. The results are also averaged to create a third transfer function appropriate for when the specimen conditions are unknown or changing.

A nonparametric system identification technique, MFDID (Kim *et al.* 1995), is used to fit the experimental transfer function data to a single-input single-output model of poles and zeros. Identified transfer function models are overlain on Fig. 8 in dashed black lines. Three pole models are found sufficient to accurately represent the dynamics over the frequency range of interest (up to 40 Hz). Models of the servo-hydraulic dynamics at 0.0 and 2.5 Amps, as well as the average of the two specimen conditions, are given by

$$G_{xu,0.0\text{A}}(s) = \frac{1.730\times10^{7}}{(s+182.7)(s^{2}+225.3s+9.499\times10^{4})} \tag{38}$$

$$G_{xu,2.5\mathrm{A}}(s)=\frac{1.613\times10^{7}}{(s+134.2)(s^{2}+324.6s+1.211\times10^{5})} \tag{39}$$

$$G_{xu,\mathrm{avgA}}(s)=\frac{1.600\times10^{7}}{(s+151.7)(s^{2}+250.4s+1.061\times10^{5})} \tag{40}$$

Fig. 8 shows that the behavior of the servo-hydraulic system is frequency dependent, where the magnitude and phase (or equivalently, the time lag) varies with frequency. Traditional delay compensation approaches based on a single constant time delay would be inadequate for systems that respond at multiple frequencies, such as MDOF structures. Likewise, traditional approaches do not address the decay in magnitude observed.

Feedforward actuator controllers are developed using both CDM and BDM approaches for each of the three specimen conditions. Whenever the specimen conditions are changing or unknown, the average controller is used (either with or without LQG feedback control). A summary of the controllers investigated is presented in Table 2.

Table 2 Actuator controllers

Method	*Specimen Conditions*	*Short Name*
CDM with Linear Acceleration Extrapolation	0.0 Amps	$G_{\mathrm{FF,0.0A}}$ CDM
	2.5 Amps	$G_{\mathrm{FF,2.5A}}$ CDM
	Average / General	$G_{\mathrm{FF,avgA}}$ CDM
	Average / General	$G_{\mathrm{FF,avgA}}$ CDM + LQG
BDM (Second Order)	0.0 Amps	$G_{\mathrm{FF,0.0A}}$ BDM
	2.5 Amps	$G_{\mathrm{FF,2.5A}}$ BDM
	Average / General	$G_{\mathrm{FF,avgA}}$ BDM
	Average / General	$G_{\mathrm{FF,avgA}}$ BDM + LQG

5.1 Actuator tracking performance in the frequency domain

To evaluate performance in the frequency domain, the actuator controllers were implemented using a sampling rate of 2000 Hz. Then, a BLWN from 0 to 50 Hz with a displacement RMS of 0.254 mm was commanded to experimentally determine the servo-hydraulic system transfer function with outer-loop control (Fig. 3). Controllers were designed to match the specimen conditions, with results for the 0.0 Amp condition in Fig. 9 and the 2.5 Amp condition in Fig. 10. Perfect controller performance would be indicated by unit magnitude, zero phase, and zero time lag.

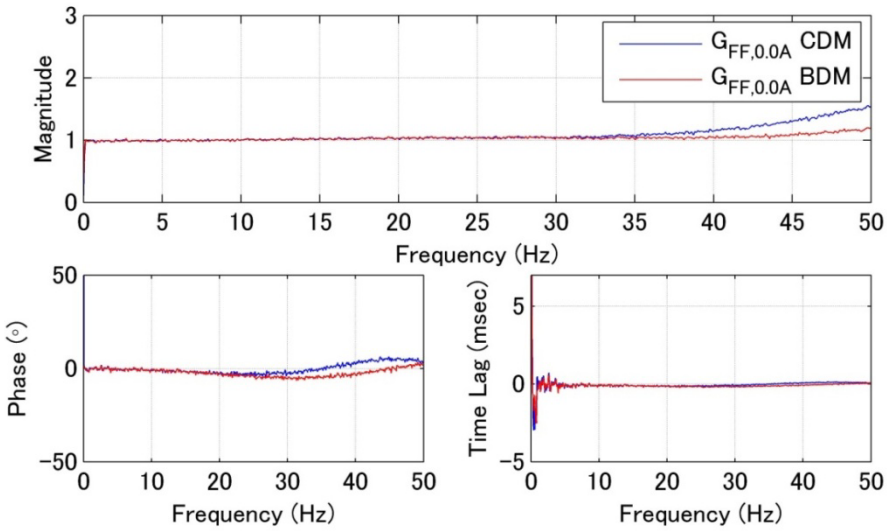

Fig. 9 Servo-hydraulic system transfer functions with 0.0 Amps in the MR damper.

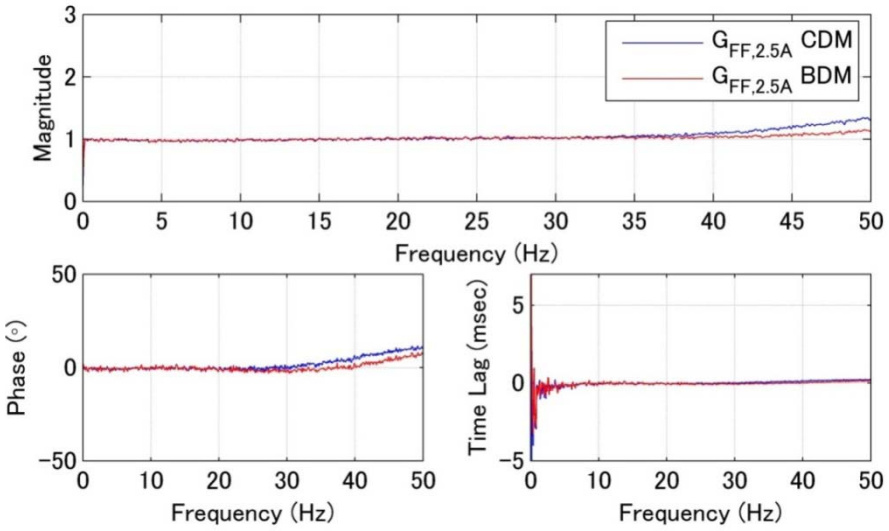

Fig. 10 Servo-hydraulic system transfer functions with 2.5 Amps in the MR damper

Both controllers offer improved bandwidth when compared to the inner-loop controller alone (Fig. 8). The feedforward controller based on the BDM provides better compensation at the higher frequencies. Over low-frequencies, both methods are similar. The result of phase and time-lag are nearly identical. This study shows that both controllers work very well, though a slight advantage in performance and simplicity is seen with the BDM.

5.2 Actuator tracking performance in the time domain

The tracking performance of the actuator in time domain is evaluated using two predefined displacements: a BLWN with a bandwidth of 0 to 5 Hz and a BLWN with a bandwidth of 0 to 15 Hz. During the predefined displacement commands, three MR damper specimen conditions are examined, including a 0.0 to 2.5 Amp pulse at 0.5 Hz and 50% duty cycle, constant 0.0 Amps, and constant 2.5 Amps. The controllers in each case are designed as using average, 0.0 Amp, and 2.5 Amp identified models, respectively. The sampling frequency is chosen as 2000 Hz. The accuracy of tracking is quantified by the RMS error norm between the desired (predefined) displacement and measured displacement, as given by

Table 3 MR Damper Tracking Performance for predefined displacement histories

Current Command	*Controller*	*RMS Error (%) 0-5 Hz BLWN*	*RMS Error (%) 0-15 Hz BLWN*
2.5 Amp Pulse	None	17.7	48.6
	$G_{FF,avgA}$ CDM	2.20	7.53
	$G_{FF,avgA}$ BDM	2.21	7.37
	$G_{FF,avgA}$ CDM + LQG	1.21	5.44
	$G_{FF,avgA}$ BDM + LQG	1.20	5.37
0.0 Amps	$G_{FF,0.0A}$ CDM	0.96	3.16
	$G_{FF,0.0A}$ BDM	0.95	3.14
	$G_{FF,avgA}$ CDM + LQG	1.15	4.11
	$G_{FF,avgA}$ BDM + LQG	1.16	4.12
2.5 Amps	$G_{FF,2.5A}$ CDM	2.51	5.32
	$G_{FF,2.5A}$ BDM	2.58	5.29
	$G_{FF,avgA}$ CDM + LQG	1.37	6.08
	$G_{FF,avgA}$ BDM + LQG	1.39	6.05

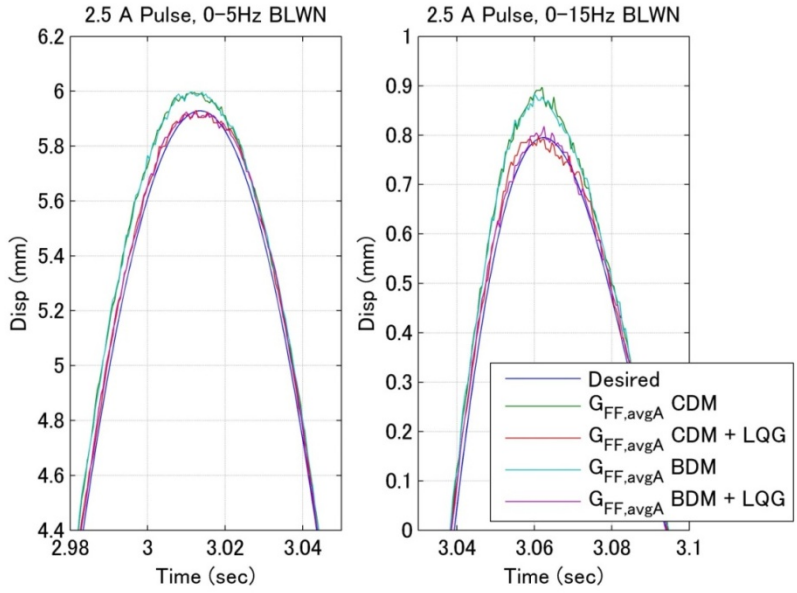

Fig. 11 Displacement tracking during a pulse in current

$$\text{RMS error (norm)} = \sqrt{\frac{\sum_{i}^{N}(r_i - y_i)^2}{\sum_{i}^{N}(r_i)^2}} \times 100\% \tag{41}$$

where N is the number of time steps, r_i is the desired displacement and x_i is the measured displacement.

5.3 Real-time hybrid simulation of 9-story benchmark structure

To verify the accuracy of the proposed model-based control method for large scale structures in RTHS, a nine-story steel frame benchmark structure is chosen (Ohtori *et al.* 1994). This structure has 5 bays in NS and EW directions. The lateral resisting system in the NS direction is examined, as shown in Fig. 12. Mass and stiffness matrices are assembled from the estimated seismic mass and structural properties, respectively. Structural control provided by MR dampers (added to the structure between the ground story and first story for this study) is assumed to keep response of the structure in the linear range for the earthquakes investigated. The first 5 natural frequencies of this structure are 0.443, 1.18, 2.05, 3.09, and 4.27 Hz, with a maximum natural frequency of 63.6 Hz for the 29th mode. Modal damping (Craig and Kurdila 2006) is used to calculate the damping matrix with 2% damping assigned to each mode. In this RTHS, the MR damper is represented by a physical specimen, while the rest of the structure is simulated numerically. The large-scale MR

damper is difficult to model numerically over the entire range of expected frequencies and amplitudes, especially in the presence of semi-active control, thus RTHS is required for accurate performance evaluation. The input earthquake investigated is the 1940 El Centro earthquake with a scale factor of 0.5. The CDM is selected for numerical integration with a sampling frequency of 2000 Hz.

Results from RTHS of the benchmark nine-story structure are presented in Fig. 13 for the MR damper in semi-active control mode. The semi-active controller is based on the clipped-optimal control algorithm (Dyke *et al.* 1996) with equal acceleration weighting on all stories paired with very low weighting of the MR damper force. The actuator controllers investigated include CDM and BDM feedforward controllers for the average specimen condition both with and without feedback control. The figure includes plots of the time histories of the displacement and force of MR damper, the ninth-story acceleration, the force-displacement hysteresis of the MR damper,and the force-velocity hysteresis of the MR damper.

To verify the accuracy of the applied displacement to the MR damper, the RMS error between desired displacement and measured displacement for each controller is calculated using Eq. (41) and the results are in summarized the Table 4. The RMS error of the controllers based on the BDM are smaller than the CDM, although both are small to begin with.

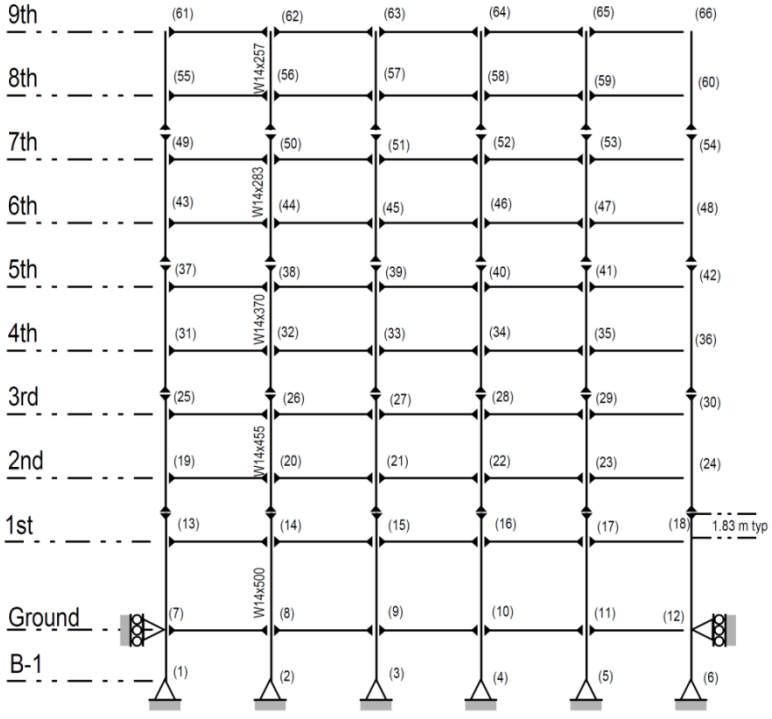

Fig. 12 nine-story benchmark structure (Ohtori *et al.*1994)

Table 4 RMS error during RTHS of the nine-story benchmark structure

Controller	*RMS Error (%)*
$G_{FF,avgA}$ CDM	0.786
$G_{FF,avgA}$ BDM	0.740
$G_{FF,avgA}$ CDM + LQG	0.577
$G_{FF,avgA}$ BDM + LQG	0.554

Table 5 Datasets from experimental studies

Experiment	*Section*	*Dataset*
System identification of servo-hydraulic system	5	Phillips *et al.* (2014a)
System identification with outer-loop control	5.1	Phillips *et al.* (2014b)
Tracking performance of outer-loop controllers	5.2	Phillips *et al.* (2014c)
RTHS of 9-story structure with MR damper	5.3	Phillips *et al.* (2014d)

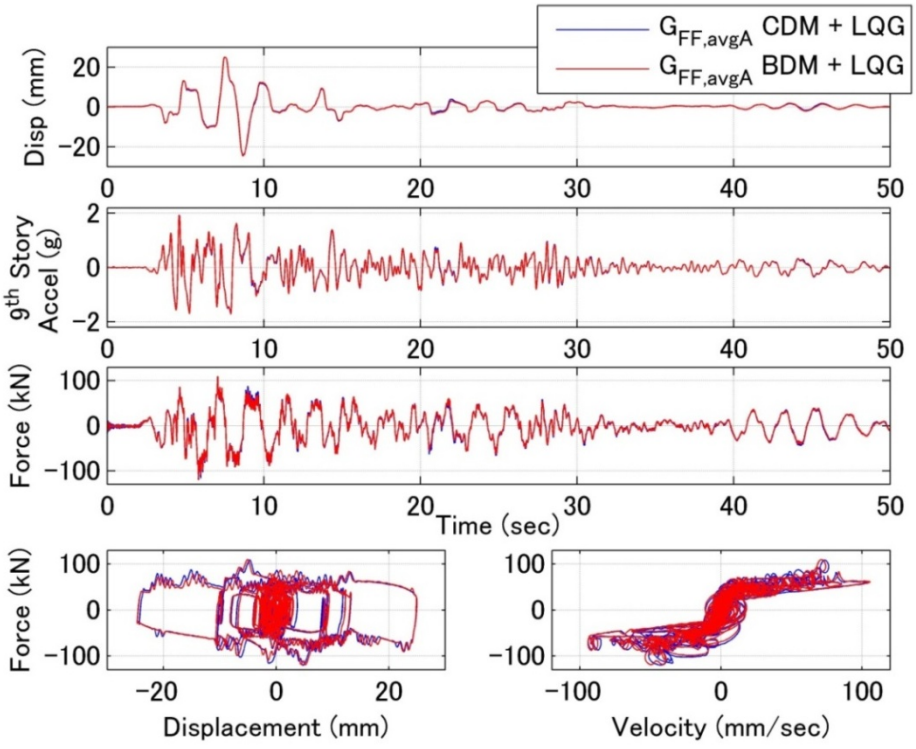

Fig. 12 MR Damper response using semi-active control

6. Conclusions

An effective approach to model-based feedforward control development for RTHS has been presented. The BDM provides an alternative to discretize an improper continuous time system by estimating the higher order derivatives. The BDM is more straightforward, provides a consistent method among derivatives, and is flexible for servo-hydraulic system models of any order.

In the frequency domain, the feedforward controller designed using the BDM performs slightly better than the CDM, especially over the high-frequency range. In time domain, both methods have a small and similar RMS error. Although both the feedforward control methods produce comparable results in RTHS, the BDM, approach provides a simpler and more flexible framework to implement potentially improper transfer functions for feedforward compensation. The results of the experimental studies can be found in the datasets listed in Table 5.

Acknowledgements

The authors would like to acknowledge the support of the National Science Foundation under award CMMI-1011534.The authors would also like to thank Richard E. Christenson for the use of the 200 kN MR damper.

References

Carlson, J.D. and Jolly, M.R. (2000), "MR fluid, foam, and elastomer devices", *Mechatronics*, **10**(4-5), 555-569.

Carrion, J.E. and Spencer Jr., B.F. (2007), *Model-based strategies for real-time hybrid testing*, Newmark Structural Engineering Laboratory Report Series, University of Illinois at Urbana-Champaign, Urbana, IL, No. 6.

Carrion, J.E., Spencer Jr., B.F. and Phillips B.M. (2009), "Real-time hybrid simulation for structural control performance assessment", *Earthq. Eng. Eng. Vib.*, **8**(4), 481-492.

Chen, C. and Ricles, J.M. (2009), "Analysis of actuator delay compensation method for real-time testing", *Eng. Struct.*, **31**(11), 2643-2655.

Craig, R.R. and Kurdila, A.J. (2006), *Fundamentals of Structural Dynamics*, 2nd Ed., Wiley, Hoboken, NJ, USA.

Dyke, S.J., Spencer Jr., B.F., Quast, P. and Sain, M.K. (1995), "Role of control-structure interaction in protective system design", *J. Eng. Mech. - ASCE*, **121**(2), 322-338.

Dyke, S.J., Spencer, Jr., B.F., Sain, M.K. and Carlson, J.D. (1996), "Modeling and control of magnetorheological dampers for seismic response reduction", *Smart Mater. Struct.*, **5**(5), 565-575.

Hakuno, M., Shidawara, M. and Hara, T. (1969), "Dynamic destructive test of a cantilever beam controlled by an analog computer", *T. Japan Soc.Civil Eng.*, **171**, 1-9 (In Japanese).

Horiuchi, T., Nakagawa, M., Sugano, M. and Konno, T. (1996), "Development of a real-time hybrid experimental system with actuator delay compensation", *Proceedings of the 11th World Conference on Earthquake Engineering*, Paper No. 660.

Jung, R.Y., Shing, P.B., Stauffer, E. and Thoen, B. (2007), "Performance of a real-time pseudodynamic test system considering nonlinear structural response", *Earthq. Eng. Struct. D.*, **36**(12), 1785-1809.

Kim, S.B., Spencer Jr., B.F. and Yun, C.B. (2005), "Frequency domain identification of multi-input, multi-output systems considering physical relationships between measured variables", *J. Eng. Mech. - ASCE*, **131**(5), 461-473.

Lin, Y.Z. and Christenson, R.E. (2009), "Comparison of real-time hybrid testing with shake table tests for an MR damper controlled structure", *Proceedings of the 2009 American Control Conference*. St. Louis, Missouri, Paper No. FrB20.4.

Mahin, S.A. and Shing, P.B. (1985), "Pseudodynamic method for seismic testing", *J. Struct. Eng. - ASCE* **111**(7), 1482-1503.

Mahin, S.A., Shing, P.B., Thewalt, C.R. and Hanson, R.D. (1989), "Pseudodynamic test method. Current status and future directions", *J. Struct. Eng. -ASCE*, **115**(8), 2113-2128.

Merritt, H.E. (1967), *Hydraulic control systems*, Wiley, New York, NY, USA.

Ohtori, Y., Christenson, R.E. and Spencer Jr., B.F. (1994), "Benchmark control problems for seismically excited nonlinear buildings", *J. Eng. Mech. -ASCE*, **130**(4), 366-385.

Phillips, B.M., Chae, Y., Jiang, Z., Spencer Jr., B.F., Ricles, J.M., Christenson, R.E., Dyke, S.J. and Agrawal A. (2010), "Real-time hybrid simulation benchmark structure with a large-scale MR damper", *Proceedings of the 5th World Conference on Structural Control and Monitoring*, Shinjuku, Tokyo.

Phillips, B.M. and Spencer Jr., B.F. (2011), *Model-based feedforward-feedback tracking control for real-time hybrid simulation*, Newmark Structural Engineering Laboratory Report Series, University of Illinois at Urbana-Champaign, Urbana, IL, No. 28.

Phillips, B.M. and Spencer Jr., B.F. (2012a), "Model-based feedforward-feedback actuator control for real-time hybrid simulation", *J. Struct. Eng. – ASCE*, **139**, 1205-1214.

Phillips, B.M. and Spencer Jr., B.F. (2012b), "Model-based multiactuator control for real-time hybrid simulation", *J. Eng. Mech. -ASCE*, **139**(2), 219-228.

Phillips, B.M., Takada, S., Spencer Jr., B.F. and Fujino, Y. (2014a), *System identification of servo-hydraulic system*, Network for Earthquake Engineering Simulation (NEES)(distributor). Dataset. DOI: 10.4231/D3ZP3W09Z.

Phillips, B.M., Takada, S., Spencer Jr., B.F. and Fujino, Y. (2014b), *System identification of servo-hydraulic system with outer-loop control*, Network for Earthquake Engineering Simulation (NEES)(distributor). Dataset. DOI: 10.4231/D3V11VK7Z.

Phillips, B.M., Takada, S., Spencer Jr., B.F. and Fujino, Y. (2014c), *Tracking performance of outer-loop controllers*, Network for Earthquake Engineering Simulation (NEES)(distributor). Dataset. DOI: 10.4231/D3Q814S4P.

Phillips, B.M., Takada, S., Spencer Jr., B.F. and Fujino, Y. (2014d), *Real-time hybrid simulation of 9-story structure with MR damper*, Network for Earthquake Engineering Simulation (NEES)(distributor). Dataset. DOI: 10.4231/D3KH0DZ9F.

Shing, P.B., Nakashima, M. and Bursi, O.S. (1996), "Application of pseudodynamic test method to structural research", *Earthq. Spectra*, **12**(1), 29-54.

Takanashi, K. *et al*. (1975), "Nonlinear earthquake response analysis of structures by a computer actuator on-line system: Part I, details of the system", *Transactions of the Architectural Institute of Japan*, University of Tokyo, Tokyo, Japan, **229**, 77-83 (In Japanese).

Takanashi, K. and Nakamura, M. (1987), "Japanese activities on on-line testing", *J. Eng. Mech*. - *ASCE*, **113**(7), 1014-1032.

Tomizuka, M. (1987), "Zero phase error tracking algorithm for digital control", *J. Dyn. Syst. Measurement Control*, **109**(3), 65-68.

Wallace, M., Wagg, D.J. and Neild, S.A. (2005), "An adaptive polynomial based forward prediction algorithm for multi-actuator real-time dynamic substructuring", *P. Roy. Soc.*, **461**, 3807-3826.

Yang, G., Spencer Jr., B.F., Carlson, J.D. and Sain, M.K. (2002), "Large-scale MR fluid dampers: Modeling and dynamic performance considerations", *Eng. Struct.*, **24**(3), 309-323.

Zhao, J., French, C., Shield, C. and Posbergh, T. (2003), "Considerations for the development of real-time dynamic testing using servo-hydraulic actuation", *Earthq. Eng. Struct. D.*, **32**(11), 1773-1794.